Hindawi Publishing Corporation
International Journal of Distributed Sensor Networks
Volume 2012, Article ID 272190, 10 pages
doi:10.1155/2012/272190

*Research Article*

# Structural Health Monitoring of a Tall Building during Construction with Fiber Bragg Grating Sensors

**D. S. Li,[1] L. Ren,[1] H. N. Li,[1] and G. B. Song[2]**

[1] *School of Civil and Hydraulic Engineering, Dalian University of Technology, 2 Linggong Road, Dalian 116024, China*
[2] *Department of Mechanical Engineering, University of Houston, Houston, TX 77204-4006, USA*

Correspondence should be addressed to D. S. Li, dsli@dlut.edu.cn

Received 29 June 2012; Accepted 22 August 2012

Academic Editor: Jeong-Tae Kim



Fiber Bragg grating sensors demonstrate a great potential as a structural health monitoring tool for civil structures to ensure structural integrity, durability, and reliability. The advantages of applying fiber optic sensors to a tall building include their immunity to electromagnetic interference and their multiplexing ability to transfer optical signals over a long distance. In the work, fiber Bragg grating sensors, consisting of strain and temperature sensors, are applied to structural monitoring of an 18-floor tall building since the date of its construction. The strain transferring rate from host material to the fiber core is discussed and the calibration of packaged fiber Bragg grating sensor is presented. The main purposes of the investigation are monitoring temperature evolution history within concrete during the pouring and curing process, measuring variation of the main column strains on the underground floor while upper 18 floors were subsequently added on, and monitoring relative displacement between two foundation blocks. Fiber Bragg grating sensors have been installed and integrated continuously for more than five months. Monitoring results of temperature and strain are presented in the paper. Furthermore, temperature lag behavior between concrete and its surrounding air is investigated.

## 1. Introduction

Structural health monitoring attracts increasing interests in civil engineering because of its potential ability to alert managing staff of a forthcoming, dangerous state of a structure in advance. In addition, structural health monitoring helps to evaluate the extent of damage and to estimate, afterwards, the structure's remaining service life once a disaster occurred [1, 2]. Among all the sensors that can be used in structural health monitoring or smart structures in the future, fiber Bragg grating (FBG) sensors stand out as the most promising sensing element. In comparison to conventional electricity-based sensors, FBG sensors exhibit many advantages including: (1) electromagnetic inference immunity and low energy loss, which is preferable in the applications of long-distance health monitoring; (2) multiplexing ability to allow for quasi-distributive monitoring of strains by one fiber; (3) high sensibility over a wide measurement range; (4) slenderness and flexibility such that added mass and stiffness to the host structure can be neglected [1, 3]. Furthermore, FBG sensors exhibit tolerance to harsh construction conditions and excellent long-term performance [4].

The past decades have witnessed an intense research effort to embed FBG sensors that monitor many types of structures, especially bridges [1, 5]. However, tall buildings are not usually monitored, especially during its construction phase [6–8]. In current investigation, a monitoring system consisting of FBG sensors was designed to monitor: (1) temperature increase within concrete due to hydration process, (2) strain variation of the main column on the underground floor due to subsequent addition of upper 18 floors, and (3) relative long-term displacement between two sinking foundation blocks. For these purposes, FBG temperature and strain sensors were bonded on the rebars of the column and the 1st floor beam before concrete pouring. The FBG sensors have operated continuously for more than five months after installation. Concrete pouring process was precisely monitored in terms of hydration course. Strain variation in the main column was recorded when upper floors were sequentially built up along with the

Figure 1: Dongsheng Garden A5 building in construction (on October 30, 2008).

temperature records inside and outside concrete. Records of temperature were also used for compensation of FBG wavelength variations during strain monitoring. Such on-site temperature and strain monitoring data could provide valuable information for future building construction.

The paper is organized as follows: the instrumented building, the monitoring system along with packaged FBG sensors and their calibration tests are described first. Monitoring results of the building are then presented in three parts: the temperature and strain in the column before the underground floor was concreted, the concrete pouring and curing process, and the long-term strain monitoring while upper floors were built up in sequence. In the follows, the temperature lag behavior between inside concrete and ambient air, and its effects on structural health monitoring are discussed. Finally, results and contributions of the paper are summarized.

## 2. Description of the Under-Construction Building and Its Monitoring System

*2.1. Dongsheng Garden A5 Building: Description and Construction.* The project under investigation is the Dongsheng Garden A5 building, located in Fushan Bay Area (Qingdao, China). The A5 building is an 18-story frame-shear wall residential building with 54.85 meters above ground. It includes one underground floor for parking, where FBG sensors were installed. The A5 building began to be constructed on April 25, 2008. Figure 1 shows that the 12th floor was being under construction on October 30, 2008 and the red downward solid arrow points FBG sensors' locations, that is, the underground floor wall and the first floor beam.

*2.2. Fundamentals of Fiber Bragg Gratings.* A Bragg grating is a permanent periodic modulation of the refractive index in the core of a single mode optical fiber, which consists of three layers: fiber core, cladding, and coating. When light transmitted in a fiber impinges upon Bragg gratings, constructive interference between the forward wave and the contra-propagating wave leads to a narrowband back-reflection of light when the Bragg (or phase match) condition is satisfied. The Bragg condition can be expressed between the central wavelength of a Bragg grating and its period by the following relationship [9]:

$$\lambda_b = 2n\Lambda, \tag{1}$$

where, $\lambda_b$, $n$, and $\Lambda$ are the central wavelength of reflected light, effective refractive index, and period of a Bragg grating, respectively.

When a Bragg grating is exposed to mechanical strains, its period is altered and thus the wavelength of reflected light changes. In general, the wavelength of the reflected light varies with applied strain as follows:

$$\frac{1}{\lambda_b}\frac{\Delta\lambda_b}{\varepsilon} = 0.78 \times 10^{-6}/\mu\varepsilon. \tag{2}$$

Moreover, the Bragg grating is also sensitive to the variation of environment temperature as,

$$\frac{\Delta\lambda_b}{\lambda_b} = \left(\alpha_f + \xi\right)\Delta T, \tag{3}$$

where, $\alpha_f = (1/\Lambda)(d\Lambda/dT)$ is the thermoelongation coefficient and $\xi = (1/n)(dn/dT)$ is the photosensitivity coefficient of the fiber. The temperature coefficient in (3) is, in total, 10.3 pm/°C for Bragg gratings with wavelength around 1550 nm [4]. Hence, structural strain can be measured by the change of reflected light wavelength once the influences of temperature are eliminated based on (3).

*2.3. Calibration Tests of Packaged FBG Sensors.* The FBGs used in this work are inscribed in Ge-doped photosensitive optical fiber using the phase mask technique [10]. The gratings are annealed for more than 7 hours at 200°C to stabilize their performance for reliable long-term monitoring and then packaged for measurement applications since naked FBGs are fragile and too delicate to be handled [1]. Figure 2(a) illustrates a steel-tube-packaged FBG strain sensor with patented techniques developed in our laboratory.

A series of tests were performed to calibrate FBG strain sensors packaged in our laboratory. An FBG strain sensor and a strain gauge were first bonded on a steel plate in parallel with cyanoacrylate adhesive. Tensile tests of the steel plate were then carried out in the material testing system shown on the right in Figure 2(b). During the calibration tests, the steel plates were loaded continuously from 0 $\mu\varepsilon$ to 1000 $\mu\varepsilon$ and then unloaded six times to ensure repeatability. The results by calibration tests thus obtained are plotted in Figure 2(b), showing the relationship between Bragg wavelength shifts and strains measured by the strain gauge. Moreover, experimental strain sensitivity of the packaged FBG strain sensor is 0.5013 $\mu\varepsilon$/pm, which agrees well with the theoretical analysis [11, 12] in the following section.

*2.4. Strain Transferring Consideration of Packaged FBG Sensors.* Conventionally, the values measured by an FBG sensor were assumed to be actual structural strains [13]. In fact, the strain measured by an FBG is different from actual host structure strain because of the difference between

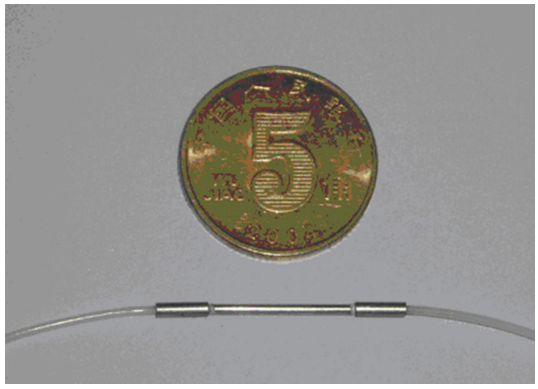

(a) Steel-tube-packed FBG sensor

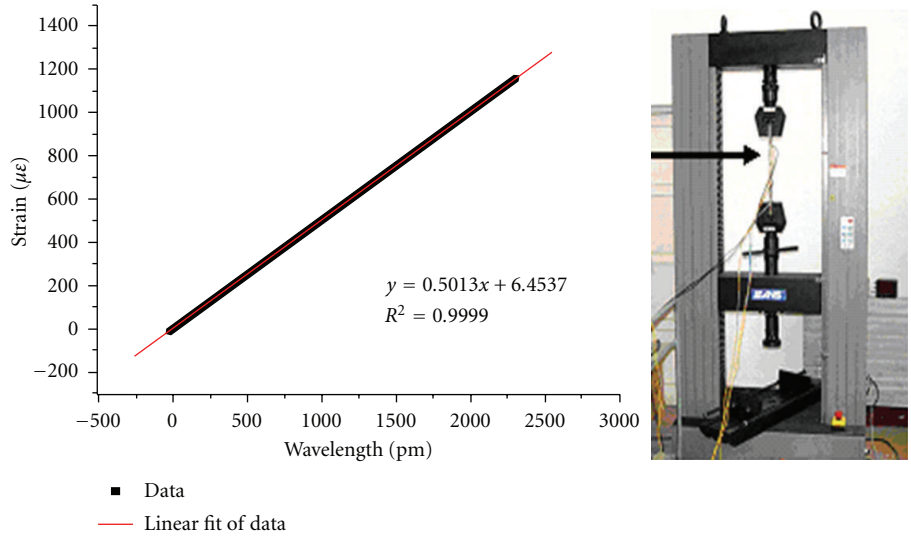


(b) Calibration tests on a universal material testing system

Figure 2: Steel-tube-packed FBG sensor and calibration tests.

the optical fiber core modulus and the modulus of the fiber coating or the adhesive. Such strain difference depends on detailed packing measures of FBGs. Generally, there are three methods to integrate FBGs with host structures in terms of packing strategies: (1) direct integration, in which FBGs are directly embedded in or surface bonded to a host structure; (2) sensor-packaging integration, by which FBGs are first fixed in a small tube or bonded on the surface of a plate, and then the tube or the plate is anchored in the host structure; (3) clamping integration, in which an FBG is gripped at two ends by a bracket fixed on the host structure. No matter how the FBGs are packaged and integrated, the fiber core is brittle and has to be protected by adhesives or a coating layer in most sensing applications to avoid fiber breakage and to ascertain its long-term stability. However, such a protection results in inconsistency between the fiber strain and the structural strain. Such discrepancies are neglected in many applications of FBGs by simply assuming that the fiber strain is consistent with the host structural strain [3, 14]. Such an assumption gives acceptable measurement results for the FBGs with long gauge length, in which the peak host strain can be fully transferred into the fiber strain, but cannot provide good measurement strains for short gauge FBGs, for instance, FBG sensors, in which the effect of the bonded fiber length on strain transfer between the fiber and host structure is significant [15]. It is, thus, of primary importance to have a detailed knowledge of the relationship between the host structural strain and the fiber strain in order to correctly interpret structural strain from the strains sensed in the fiber. For the packaged FBG sensor used in our investigation, strain transferring loss between an FBG and its external layer can be approximately written as [16, 17]

$$\varepsilon_g(x) = \varepsilon_m\left(1 - \frac{\cosh(kx)}{\cosh(kL)}\right), \tag{4}$$

where $\varepsilon_g$ and $\varepsilon_m$ are fiber core and host structural strains, respectively. $k$ is a strain lag parameter, containing both effects of the geometry and the relative stiffness on the packaging components, and can be written as

$$k^2 = \frac{2G_c}{r_g^2 E_g \ln\left(r_m/r_g\right)} = \frac{1}{(1+\nu)\left(E_g/E_c\right) r_g^2 \ln\left(r_m/r_g\right)}, \tag{5}$$

where $E_g$ and $E_c$ are Young's modulus of the optical fiber and coating layer, respectively. $G_c$ is the shear Young's modulus

of the coating or outerlayer. $r_g$ and $r_m$ are radii of the optical fiber and coating layer, respectively. $\nu$ is the Poisson's ratio of the fiber core.

Furthermore, local enhancement may occur, which necessitates the need for calibration of FBG sensors to obtain actual structural strains as shown in Section 2.3. Previous investigations indicate that the strain distribution of the host material surrounding the fiber is influenced by the fiber embedment and that the characteristics of the host material have important effects on the strain transferring from host material to fiber. The mechanical properties of the host material must, therefore, be taken into account when exploring the strain transferring from host material to the fiber. Interested readers may consult the references [18, 19] which discuss related issues in further details.

*2.5. FBG Monitoring System: Design and Installation.* We had measured vibration of a pipeline model with steel-tube-packaged FBG sensors [11, 12] and performed investigations on health monitoring of an offshore platform (number CB271, located in the Bohai Sea, China) with packaged FBG sensors bonded on the circumference of the pillar [11, 12]. With the three objectives outlined in the Introduction and with reference to the experience gained from previous investigations, a monitoring system consisting of packaged FBG sensors with adequate protection measures was designed. The monitoring system involves initially seven FBG sensors.

In a later stage, another FBG temperature sensor was added. Among the eight FBG sensors, four FBG strain sensors are intended to measure column strain while the building was still in construction. Two of the four FBG strain sensors were bonded on the rebars of the upper part of the column, 40 cm below the beam as illustrated in Figure 3(a), and the other two on the lower part of the column, about 50 cm above the underground floor as shown in Figure 3(b). Another two FBG strain sensors were adhered to the horizontal beam as shown in Figure 3(c) to monitor relative displacements between two foundation blocks. As far as temperature is concerned, two FBG sensors were installed. One sensor (FBG 7#) was left freely in a plastic pipe between rebars to measure temperature variation inside concrete, whereas the other (FBG 8#) was laid in the junction box (not shown in the figure) to measure environment air temperature as shown in Figure 3(d). All the eight FBG sensors were located directly underneath the standing worker wearing a blue suit in Figure 4(a).

The eight FBG sensors were multiplexed serially into two single-mode optical fibers (Figure 3(d)), which were protected in plastic pipes as shown in Figure 4(b) and routed to the monitoring room around 100 meters away. The acquisition system was composed of a demodulation unit FBG-SI425 (Micronoptics Incorporated), a personal computer, and a digital interface PCMCIA card. A customized program running under LABVIEW (National Instruments) on the PC was developed for acquiring data every minute from the FBG sensors through FBG-SI425 and the PCMCIA card. The acquired data are then saved in separate files automatically. The sampling interval can be adjusted for desired frequency to accommodate the requirement of various construction phases.

Table 1: Daily temperature variation before concreting.

| Date (July, 2008) | 7.14 | 7.15 | 7.16 | 7.17 | 7.18 | 7.19 |
|---|---|---|---|---|---|---|
| Lowest temperature (°C) | 22.5 | 23.5 | 20.9 | 22 | 22.9 | 23.2 |
| Highest temperature (°C) | 25 | 25.2 | 26.7 | 27.7 | 24.6 | 26.3 |
| Maximum difference (°C) | 2.5 | 1.7 | 5.8 | 5.7 | 1.7 | 3.1 |

As pointed out in previous paragraphs, FBG sensors need to be protected from concrete aggregate during cement pouring. Details of FBG sensors' fixture to the rebars and their protection in the investigation are illustrated in Figures 3 and 4. Packaged FBG sensors were first bonded to the rebars with epoxy, and then wrapped with gauze patches to allow for solidification of the epoxy. In addition, steel hoses were presleeved to shield leadings of bonded FBG sensors (small silver steel hoses shown in Figure 3) and plastic pipes (large blue ones) were used to house optical fibers. Moreover, two junction boxes are placed in the wall to (1) protect optical connectors, (2) to check the integrity of each FBG sensor, and (3) to provide long-term monitoring once the building is completed. Furthermore, larger and harder pipes were used to protect communication fibers leading to the monitoring room as shown in Figure 4.

## 3. Dongsheng Garden A5 Building Monitoring Results

The monitoring of strain and temperature of the A5 building during construction can be categorized into three periods: the first is around one-week before concreting of the 1st floor; the second is immediately followed by concrete pouring and includes curing process which lasts approximately 10 days; and finally the long-term monitoring with upper 18 floors built up sequentially.

*3.1. One-Week Monitoring before Cement Pouring.* After one week of sensor installation, the monitoring of temperature and rebar strain started. Figure 5 shows the time history of two FBG strain sensors bonded on the upper rebars of the column (FBG 3# and FBG 4# as shown in Figure 3(a)). The blue solid curve and the red dotted curve illustrate the strain variation measured by FBG 3 and FBG 4, respectively. Both rebars belong to the same column and are supposed to bear similar loads. The first parts of the curves in Figure 5 demonstrate clearly that both FBG sensors were synchronously stressed with respect to the strains measured at 00:00:00 on July 14, 2008. However, FBG 3 sensor measured 15 $\mu\varepsilon$ compressive strains more than that measured by FBG 4 between July 18 and July 20. It is postulated that the workers may have unevenly laid construction materials on the column during the three days, and that the rebars were subjected to unequal loads due to loose connections in-between. The rebars display, therefore, asynchronous strain variations. Nevertheless, no visual evidence was available to confirm such an argument.

(a) Two rebars in the 1st floor horizontal beam bonded with FBG sensors; top: FBG 1#, 1529 nm; bottom: FBG 2#, 1564 nm

(b) Lower part of two rebars in the vertical underground column bonded with FBG sensors; left: FBG 5#, 1557 nm; right: FBG 6#, 1525 nm

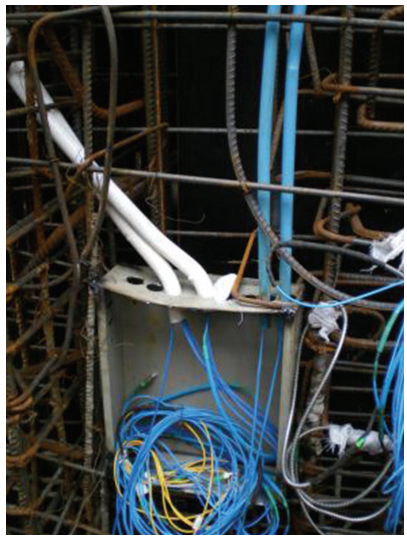

(c) Junction box with two FBG sensors; FBG 7#, 1519 nm; FBG 8#, 1548 nm

(d) Upper part of two rebars in the vertical underground column bonded with FBG sensors; left: FBG 3#, 1534 nm; right: FBG 4#, 1562 nm

Figure 3: Installation of the FBG sensors, their position, and protection measures on site.

(a) Layout of the first floor and shear wall of the A5 building installed with FBG sensors (sensors bonded on the rebars underneath the standing worker)

(b) Plastic pile protecting the connection fibers leading to the monitoring room

Figure 4: Installation of the FBG sensors, their protection, and routing to the monitoring room.

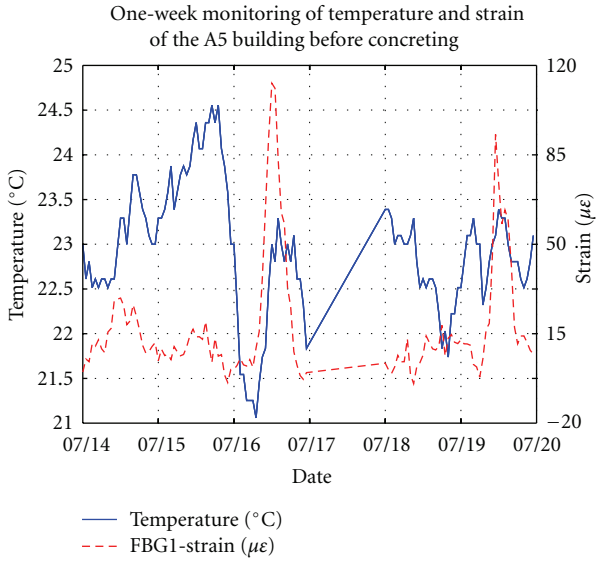


Figure 5: One-week monitoring of column strains of the A5 building before concreting.

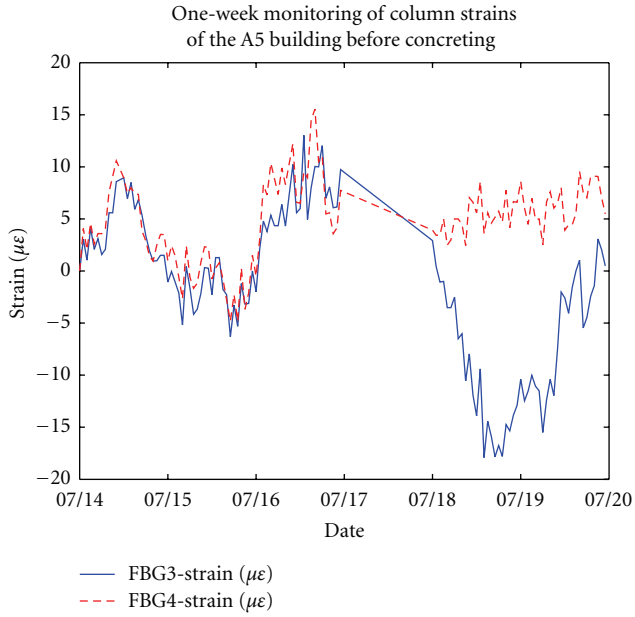


Figure 6: Strain and temperature variations in the beam rebar on the first floor before the concreting.

The strains in the 1st floor beam and the temperatures in the rebars before concreting were monitored as shown in Figure 6. The blue solid curve represents the change in temperature within 4°C. For the purpose of comparison, daily temperature records, which were obtained from the Qingdao Weather Bureau (http://qdqx.qingdao.gov.cn/), are listed in Table 1. It can be clearly observed that measured temperatures (shown in Figure 6) agree well with the records (Table 1). Furthermore, the temperature record on July 14 was also used to adjust relative temperatures measured by the FBG temperature sensor in the investigation. It should be noted that the rebars, junction boxes, and the protection

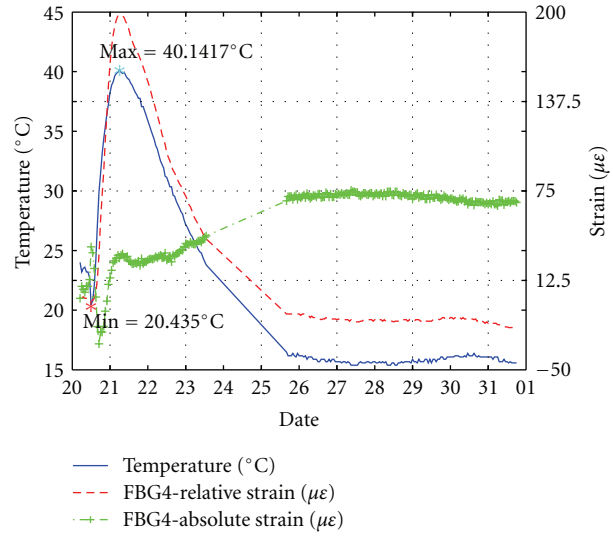


Figure 7: Strain and temperature variations during the concrete pouring and curing in the column.

pipes are hidden in the shadows. Therefore, the temperatures measured by the FBG sensor in Figure 6 are slightly lower than the local air temperature.

The red dashed curve in Figure 6 illustrates the strains measured by the FBG 1 sensor. Two obvious peaks appeared with maximum strains of 110 $\mu\varepsilon$ and 90 $\mu\varepsilon$. It was later verified that construction materials and working apparatus were placed on the horizontal beam temporarily, where the FBG 1 sensor is located. Unfortunately, a construction worker was unaware of the fragility of FBG sensors and accidentally broke one lead of the FBG 1 sensor during the installation, which resulted in the unavailability of the FBG 1 sensor in further measurements.

*3.2. Concrete Pouring and Curing.* During the pouring of concrete into the beam of the first floor and the column of the underground floor where optical sensors were located, FBG sensors were integrated every minute to ensure that variation of temperature and strain inside cement could be accurately traced with a proper frequency. Figure 7 illustrates temperature variations recorded by the optical temperature sensor during concrete pouring and initial curing with time. The horizontal axis denotes the date starting from July 20 to August 1, 2008. At 04:00:00, July 20, 2008, which is the starting time of Figure 7, environment air temperature was 24°C. The blue solid curve illustrates the temperature evolution ranging from the minimum of 10.435°C to the maximum of 40.1417°C. In the graph, three phases are clearly distinguishable: the first is the fresh concrete (phase I); followed by a quick-rising phase (phase II), and finally there is a temperature-decreasing trend and a long stabilization process (phase III).

The reason for the temperature decrease in the first phase may be attributed to the fact that the temperature of fresh cement with much water content was lower than that of embedded FBG sensors, which experienced originally environment air temperature. Once the optical temperature

Table 2: Concrete pouring date floor by floor.

| Floor number | Concreting date | Lowest temperature (°C) | Highest temperature (°C) | Maximum difference (°C) |
|---|---|---|---|---|
| 1 | 8.25 | 21.5 | 26.9 | 5.4 |
| 2 | 9.4 | 21.1 | 24.9 | 3.8 |
| 3 | 9.12 | 19.2 | 28.7 | 9.5 |
| 4 | 9.19 | 23 | 25.8 | 2.8 |
| 5 | 9.27 | 11.8 | 19.5 | 7.7 |
| 6 | 10.3 | 18.5 | 24.3 | 5.8 |
| 7 | 10.8 | 15.5 | 20.6 | 5.1 |
| 8 | 10.14 | 17.1 | 23.4 | 6.3 |
| 9 | 10.19 | 16.3 | 23.7 | 7.4 |
| 10 | 10.25 | 11.9 | 19.1 | 7.2 |
| 11 | 10.31 | 11.2 | 16.8 | 5.6 |
| 12 | 11.5 | 15.6 | 20.4 | 4.8 |
| 13 | 11.10 | 4.1 | 11.6 | 7.5 |
| 14 | 11.16 | 5.7 | 12.9 | 7.2 |
| 15 | 11.21 | 4.9 | 12.8 | 7.9 |
| 16 | 11.26 | 5.8 | 11.8 | 6 |
| 17 | 12.1 | 8.5 | 14.7 | 6.2 |
| 18 | 12.7 | 1.2 | 7.5 | 6.3 |

sensor was totally immersed in the cement while the pouring continued, its temperature decreased. As the concrete began to cure shortly after the pouring was finished, a rapid increase in the temperature was observed due to exothermic reaction of cement in the second phase, which lasted about 16 hours. The temperature rise was then followed by a gradual decreasing course in the third phase, which lasted more than 7 days. Finally, the temperature in the concrete stabilized at a constant level in the third stage, and the curing process ceased.

Strain variation during the pouring and curing of concrete in the steel-frame wall by a typical strain sensor (FBG 4) was presented by the red dashed line in Figure 7. Recall that the FBG 4 strain sensor is attached to the column rebar with a calibrated wavelength of 1562 nm as shown in Figure 3(a). The right vertical axis shows that strain variation of the FBG 4 sensor ranges from $-21.5\,\mu\varepsilon$ to $197.5\,\mu\varepsilon$. The trend of strain variation of concrete follows exactly the temperature changes, which indicates that the strain measured in concrete was mainly attributed to the thermal expansion and contraction of concrete, but not to external forces. The initial compressive strain measured by the FBG strain sensor was due to thermal contraction of the steel rebar immersed in fresh concrete.

It is well known that FBG sensors have cross sensitivities with both strain and temperature. In Figure 7, the green dash-dotted line represents the "absolute strain" measured by the FBG strain sensor due to external forces, that is, the strain induced by the temperature variations is already eliminated with the calibrated sensitivities (shortened for naming convenience, "total strain minus thermal strain" is more appropriate). It is interesting to note that tensile strains were measured by the FBG sensor and the rebar was elongated in the first phase. This may attribute to the flowing of cement below the FBG sensor and the rebar enduring temporary tensile stress. Immediately after that, compressive strain was measured. Apparently, the compressive strain was caused by the weight of the cement on the rebar. After the compression phase, tensile strains were recorded.

It is noteworthy that the period between 13:00 on July 23 and 16:00 on July 25, 2008 was due to lack of measurement data because of power breakdown onsite. The construction site was far from downtown and electric power facilities were not well maintained. Nevertheless, the unavailable measurement data shown in Figure 7 were compensated with straight lines by two nearby measurements without interpolation. In the following figures, the same rules are applied if not stated otherwise. Furthermore, although the workers were aware that the sensors are present in the framework, they did not take additional precautions during concreting, and poured directly and vibrated. All but two of the installed sensors were working properly after concreting. One sensor was lost at just the beginning of concreting, and the other was active for the first several hours, but lost its signal a little later.

*3.3. Long-Term Construction Monitoring with Added Building Floors.* Influences of the construction of upper building floors on the underground column were investigated in this subsection. The strains on the column rebars were continuously and remotely monitored in the monitoring room. The sampling interval is one hour, which was not as frequent as the previous section. Measurements obtained by the sensors are presented in Figure 8. The blue solid curve in Figure 8 illustrates measured temperature variation for a period of approximately half a year. In the graph, the dates with available monitoring data when the power was not broken down are indicated. The red dashed curve presents the strain variation in the concrete column, and it could be clearly observed that the strain follows roughly the same trend as that of temperature. The build-up of compressive strains was due to the construction of different building floors. Dates of concrete pouring of different floors were listed in the 2nd column of Table 2. The construction of the ground floor took place 35 days after the pouring of concrete into the underground wall. Concrete pouring began on August 25 and was completed on December 7, 2008. The 3rd and 4th columns show also the environment temperature, which will be used later in the subsequent section to compare the temperature difference inside and outside the concrete.

Furthermore, the column strains on pouring dates of the upper floors clearly show valleys, which was apparently caused by the adding weights of the poured concrete. On the other hand, strain anomalies were also detected, which could be explained by the short gauge length of the FBGs used for the optical sensors (approximately 10 mm) that could result in the measurement of localized strains at the sensor positions. In the future, long gauge FBG strain sensors may be developed to accommodate such demands [8].

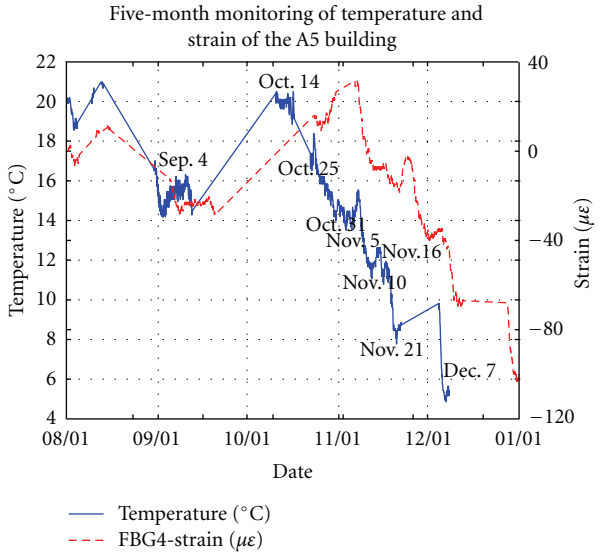


Figure 8: Strain and temperature variations in the five-month's monitoring of the A5 building.

## 4. Temperature Lag between Inside the Concrete and Environment

*4.1. Validate Measured Temperature by the FBG Sensors.* To validate measured temperatures in concrete, environment air temperature of the local area, especially daily temperature records on concrete pouring dates of different floors, was obtained from the Qingdao Weather Bureau and listed in the last three columns of Table 2. The 3rd column of Table 2 lists the lowest temperature whereas the 4th column lists the highest temperature. Since the construction site is not far from the city center and actual on-site air temperatures were not measured, the temperature records in Table 2 can be reasonably regarded as the Dongsheng A5 building on-site air temperature without much deviation.

Figure 9 illustrates measured concrete temperature by the FBG 8 temperature sensor, which was located in the junction box on the wall of the underground floor as shown in Figure 3(c). The lowest temperatures are drawn by the green dash-dotted line whereas the highest temperatures by the red dashed line in Figure 9. Due to frequent breakdowns of power on the construction site, the measurements are not completely continuous. Nevertheless, it could be clearly observed that measured concrete temperatures by the FBG 8 sensor fall well within the temperature range. The FBG 8 sensor is, therefore, considered to be capable of monitoring concrete temperature adequately.

*4.2. Temperature Lag between Concrete and Environment.* It is known that the temperature inside concrete lags normally behind the temperature of its surrounding environment. Concrete takes a while to warm up or cool down due to thermal inertia effects [20, 21]. The lagging behavior will be of great importance in structural health monitoring since structural dynamic features used for damage identification will be heavily influenced by environment temperature. For

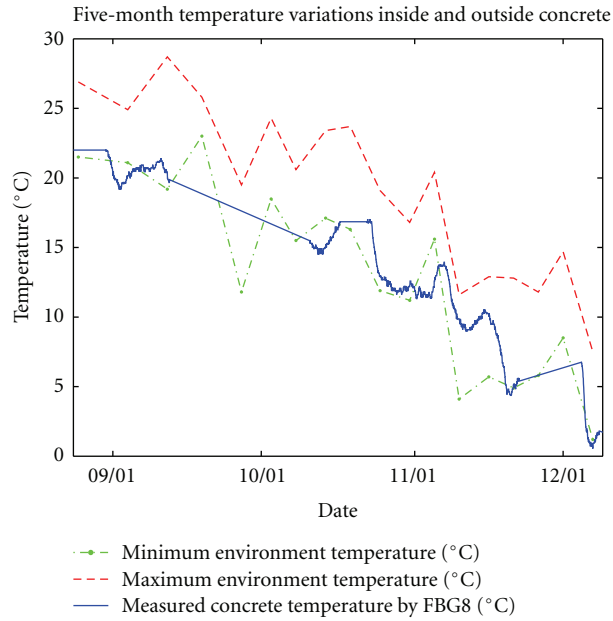


Figure 9: Environment lowest and highest temperature variations on the concrete pouring dates along with measured inside concrete temperature by the FBG 8 temperature sensor.

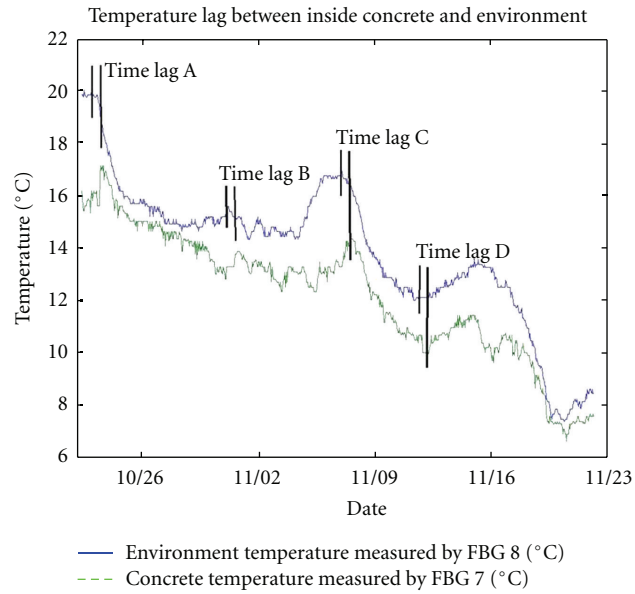


Figure 10: Comparison of inside and outside concrete temperature.

meaningful interpretations of damage index changes, temperature effects have to be eliminated. Two FBG temperature sensors installed in the Dongsheng A5 building, one inside and the other outside concrete, allows us to study this interesting temperature lag behavior.

Figure 10 takes a closer look at measured temperatures by both FBG temperature sensors in a month: FBG 8 in the junction box to measure environment temperature while FBG 7 buried in the concrete to monitor inner concrete temperature. As indicated by "time lag A", "time lag B", "time lag C" and "time lag D" in Figure 10, time lags obviously

exist between the blue solid line (environment temperature by measured FBG 8) and the green dashed line (concrete temperature by measured FBG 7). The average time lag is approximately half a day, that is, about 12 hours. This delay period agrees with the investigations by [22]. It is noteworthy that such temperature lag is strongly influenced by the dimensions of the structure, especially the thickness of the concrete. In our case, the thickness of the concrete wall is 200 mm and the FBG temperature sensor is located around 80 mm below the wall surface. Moreover, the FBG 8 sensor was laid freely in the conjunction box with only a thin wood covering. Therefore, it is believed that the FBG 8 sensor could accurately measure underground air temperature of the Dongsheng A5 building. On the other hand, the FBG 7 sensor is packaged inside a steel tube and protected by a plastic pipe as illustrated in Figure 4(b). It is therefore conjectured that there may exist a pocket of air surrounding the FBG 7 sensor, which may further increase the lagging of sensed concrete temperature with respect to external environmental temperature.

Daily temperature fluctuations could be obviously seen in Figure 10 in a 24-hour base. However, it should be noted that day temperature did not differs much from night temperature since the measured concrete wall is in the underground and because Qingdao is a seaside city. As shown in Table 2, air temperature difference between day and night in Qingdao stays mostly within 5°C, less than 10°C in extremities. This explains why the temperature in Figure 10 varies only slightly in a day and night cycle as observed in a month from October 22 to November 22, 2008. Furthermore, the downward trend clearly shows seasonal temperature variation in autumn.

## 5. Concluding Remarks

Fiber Bragg grating (FBG) sensors were used to monitor strain and temperature of a tall building while in construction; namely, three periods are monitored: before the concrete pouring, during the pouring and curing of concrete, and the construction of subsequent upper floors of the building. For this purpose, a monitoring system consisting of packaged FBG sensors with patented design in our laboratory for high and accurate strain transferring was designed. Moreover, measures were taken to protect the FBG sensors and the communication optical fibers for successful sensing. The temperature changes in the concrete during pouring and curing exhibit clearly three phases. More than five months' monitoring of the Dongsheng A5 building construction in progress permitted us to have a thorough understanding of loading variations of the main column on the underground floor.

Furthermore, structural health monitoring has generally been considered as a reliable method for determining health state of a structure. However, experience has shown that in some cases the deviation between structural temperature and environment temperature can be quite significant. It appears that temperature lag affects the effectiveness of structural health monitoring and has substantial implications in actual applications. In this investigation, the temperature lagging between inside and outside the concrete is studied and the lag time is found to be around 12 hours, which may provide interesting clues for further investigations. Moreover, the strain-transferring mechanism from neighbouring packaging material to the FBG and the influence of host material is discussed.

## Acknowledgments

The authors are grateful for the assistance of the construction workers at the Dongsheng construction site and the support of the Science Fund for Creative Research Groups of the National Natural Science Foundation of China (Grant no. 51121005) and of the Fundamental Research Funds for the Central Universities (Grant no. DUT11LK35).

## References

[1] H. N. Li, D. S. Li, and G. B. Song, "Recent applications of fiber optic sensors to health monitoring in civil engineering," *Engineering Structures*, vol. 26, no. 11, pp. 1647–1657, 2004.

[2] Y. Q. Ni, Y. Xia, W. Y. Liao, and J. M. Ko, "Technology innovation in developing the structural health monitoring system for Guangzhou New TV Tower," *Structural Control and Health Monitoring*, vol. 16, no. 1, pp. 73–98, 2009.

[3] E. Udd, "Fiber optic smart structures," *Proceedings of the IEEE*, vol. 84, no. 6, pp. 884–894, 1996.

[4] B. Culshaw and M. de Vries, *Smart Structures and Materials*, vol. 36 of *Optical Engineering*, 1997.

[5] R. C. Tennyson, A. A. Mufti, S. Rizkalla, G. Tadros, and B. Benmokrane, "Structural health monitoring of innovative bridges in Canada with fiber optic sensors," *Smart Materials and Structures*, vol. 10, no. 3, pp. 560–573, 2001.

[6] Y. Q. Ni, B. Li, K. H. Lam et al., "In-construction vibration monitoring of a super-tall structure using a long-range wireless sensing system," *Smart Structures and Systems*, vol. 7, no. 2, pp. 83–102, 2011.

[7] Y. Ni, P. Zhang, X. Ye, K. Lin, and W. Liao, "Modeling of temperature distribution in a reinforced concrete supertall structure based on structural health monitoring data," *Computers & Concrete*, vol. 8, no. 3, pp. 293–309, 2011.

[8] Y. Xia, Y. Q. Ni, P. Zhang, W. Y. Liao, and J. M. Ko, "Stress development of a supertall structure during construction: field monitoring and numerical analysis," *Computer-Aided Civil and Infrastructure Engineering*, vol. 26, no. 7, pp. 542–559, 2011.

[9] A. D. Kersey, M. A. Davis, H. J. Patrick et al., "Fiber grating sensors," *Journal of Lightwave Technology*, vol. 15, no. 8, pp. 1442–1463, 1997.

[10] K. O. Hill and G. Meltz, "Fiber Bragg grating technology fundamentals and overview," *Journal of Lightwave Technology*, vol. 15, no. 8, pp. 1263–1276, 1997.

[11] L. Ren, H. N. Li, J. Zhou, D. S. Li, and L. Sun, "Health monitoring system for offshore platform with fiber Bragg grating sensors," *Optical Engineering*, vol. 45, no. 8, Article ID 084401, 2006.

[12] L. Ren, H. N. Li, J. Zhou, L. Sun, and D. S. Li, "Application of tube-packaged FBG strain sensor in vibration experiment of submarine pipeline model," *China Ocean Engineering*, vol. 20, no. 1, pp. 155–164, 2006.

[13] C. S. Baldwin, T. Salter, J. Niemczuk, P. Chen, and J. Kiddy, "Structural monitoring of composite marine piles using multiplexed fiber Bragg grating sensors: in-field applications," in *Proceedings of the Smart Structures and Materials 2002: Smart Systems for Bridges, Structures, and Highways (SPIE '02)*, vol. 4696, pp. 82–91, San Diego, Calif, USA, March 2002.

[14] E. J. Friebele, C. G. Askins, A. B. Bosse et al., "Optical fiber sensors for spacecraftapplications," *Smart Materials and Structures*, vol. 8, pp. 813–838, 1999.

[15] C. Galiotis, R. J. Young, P. H. J. Yeund, and D. N. Batchelder, "Thestudy of model polydiacetylene/epoxy composites Part 1: the axial strain in the fibre," *Journal of Materials Science*, pp. 3640–3648, 1984.

[16] D. Li, H. Li, L. Ren, and G. Song, "Strain transferring analysis of fiber Bragg grating sensors," *Optical Engineering*, vol. 45, no. 2, Article ID 024402, 2006.

[17] H. N. Li, G. D. Zhou, L. Ren, and D. S. Li, "Strain transfer coefficient analyses for embedded fiber bragg grating sensors in different host materials," *Journal of Engineering Mechanics*, vol. 135, no. 12, pp. 1343–1353, 2009.

[18] W. Y. Li, C. C. Cheng, and Y. L. Lo, "Investigation of strain transmission of surface-bonded FBGs used as strain sensors," *Sensors and Actuators A*, vol. 149, no. 2, pp. 201–207, 2009.

[19] K. T. Wan, C. K. Y. Leung, and N. G. Olson, "Investigation of the strain transfer for surface-attached optical fiber strain sensors," *Smart Materials and Structures*, vol. 17, no. 3, Article ID 035037, 2008.

[20] G. Kister, D. Winter, Y. M. Gebremichael et al., "Methodology and integrity monitoring of foundation concrete piles using Bragg grating optical fibre sensors," *Engineering Structures*, vol. 29, no. 9, pp. 2048–2055, 2007.

[21] R. D. Nayeri, S. F. Masri, R. G. Ghanem, and R. L. Nigbor, "A novel approach for the structural identification and monitoring of a full-scale 17-story building based on ambient vibration measurements," *Smart Materials and Structures*, vol. 17, no. 2, Article ID 025006, 2008.

[22] C. Liu and J. T. DeWolf, "Effect of temperature on modal variability of a curved concrete bridge under ambient loads," *Journal of Structural Engineering*, vol. 133, no. 12, pp. 1742–1751, 2007.